Adsorption 10: 5–18, 2004

Structural and Adsorptive Characteristics of Pyrocarbon/Silica Gel Si-60

V.M. GUN'KO AND V.V. TUROV
Institute of Surface Chemistry, 17 General Naumov Street, 03164 Kiev, Ukraine

J. SKUBISZEWSKA-ZIĘBA, B. CHARMAS AND R. LEBODA
Faculty of Chemistry, Maria Curie-Sklodowska University, 20031 Lublin, Poland

Received August 15, 2001; Revised June 23, 2003; Accepted September 5, 2003

Abstract. Pyrocarbon/silica gel adsorbents (carbosils, CS) with mesoporous Si-60 (Merck, granule size 0.2–0.5 mm) modified by pyrolysis of CH_2Cl_2 at 823 K and reaction time from 0.5 to 6 h and then hydrothermally treated at 473 K for 6 h were studied by means of TEM, adsorption and ^{1}H NMR methods. Changes in the structural and adsorptive characteristics of hybrid adsorbents before and after hydrothermal treatment, which depend on pyrocarbon content (C_C), were analyzed on the basis of TEM micrographs and *p*-nitrophenol and nitrogen adsorption isotherms treated using a constrained regularization method. Interfacial water layers in aqueous suspension of CS were investigated by means of ^{1}H NMR with freezing-out of bulk water at $T < 273$ K showing nonlinear changes in the Gibbs free energy of interfacial water with increasing C_C because of nonlinear dependence of the structural characteristics of pyrocarbon deposits and CS as a whole on C_C.

Keywords: mesoporous silica gel, pyrocarbon/silica gel, nitrogen adsorption, pore size distribution, *p*-nitrophenol adsorption, interfacial water, ^{1}H NMR, Gibbs free energy

1. Introduction

Carbon-mineral materials typically possessing mosaic surfaces with carbon and mineral patches can be applied for different purposes (Leboda, 1992, 1993; Kamegawa and Yoshida, 1990, 1993, 1995; Dabrowski and Tertykh, 1996; Fenelonov, 1995). Adsorptive features of such hybrid adsorbents depend on the nature of a support and a carbonized organic precursor and conditions of pyrolysis, which determine the morphology of adsorbents, the accessibility of oxide and carbon patches, and the availability of different acidic and basic surface sites. With elevating temperature $T_{pyr} > 1000$ K and time of the pyrolysis, enlargement of graphenes and their overlapping take place, and they form a pregraphite lattice. If $T_{pyr} < 1000$ K that large graphite planes do not grow, as the formation of a turbostratic structure is a final stage of the carbonization, and pyrocarbon deposits possess a structure akin to that of carbon black. If the carbonization time is short that a disordered carbon layer forms on a support surface and the size of pyrocarbon grains does not exceed several nanometers (Fenelonov, 1995; Leboda, 1992). The morphology of pyrocarbon deposits depends also on the activity and the distribution of surface sites on the support (e.g., individual and mixed oxides) or heterogeneous sites (metal or metal oxide clusters and crystallites) formed during pyrolysis of such precursors as metal acetylacetonates (Gun'ko et al., 2000a–d, 2002 c,d).

It is known (Kiselev and Lygin, 1972; Dabrowski and Tertykh, 1996; Legrand, 1998) that both thermal and hydrothermal treatments (HTT) of silica gels change their texture, namely HTT reduces the specific surface area and enhances the pore size depending on the treatment temperature and time. Clearly, marked structural alterations in the silica matrix can occur during pyrolysis of organics at 700–1000 K depending on the

nature of reactants, especially if water is one of the products of carbonization (Gun'ko et al., 2000a–d, 2001b, 2002c,d). It should be noted that the influence of hydrothermal treatment of hybrid carbon/mineral adsorbents on their texture is inadequately investigated, as well as the impact of the chemical composition of carbonized organics on the structural parameters of hybrid adsorbents. The textural and adsorptive characteristics of carbon/silica (carbosil, CS) surfaces have been studied using a variety of physicochemical methods (Leboda, 1992, 1993; Kamegawa and Yoshida, 1990, 1993, 1995; Villieras et al., 1998; Gun'ko et al., 2000a–d, 2001b, 2002c,d). Despite these investigations, the relationships between the structural characteristics of different phases of hybrid adsorbents and their influence on adsorption of polar and nonpolar compounds are unclear in a significant part because of a variety of pyrocarbon deposits, the complexity of their morphology, and the availability of different active surface sites on both pyrocarbon and support phases. Therefore, the aim of this paper is to characterize the structural and adsorptive properties of pyrocarbon/silica gel Si-60 initial and after HTT depending on carbon content by means of nitrogen, *p*-nitrophenol (PNP) and water adsorption, TEM, and ^{1}H NMR methods.

2. Experimental Section

2.1. Materials

Mesoporous silica gel Si-60 (Merck, grain fraction 0.2–0.5 mm) was used as the initial material. Si-60 was heated in the nitrogen stream at 823 K for 6 h (labeled Si-60-T) to compare with carbosils prepared by pyrolysis of CH_2Cl_2 (purity 99%, Polish Chemical Reagent Factory) at Si-60 (10 g) under dynamic conditions in a flow rotary quartz reactor with the deoxidized nitrogen stream (100 cm^3/min) at 823 K for 0.5, 1, 2, 3, 4, and 6 h (labeled CS-i at $i = 1$–6). The rate of liquid CH_2Cl_2 feeding to the reactor (through a glass evaporator heated at 373 K) was 0.6 cm^3 min^{-1} using a Masterflex (Cole Parmer) pump. The carbon content (C_C) in CS-i was 1.5, 2.3, 5.9, 10, 13, and 19.5 wt.%, respectively, determined using differential thermal analysis on heating of samples in air from 293 K to 1273 K using a Derivatograph C (Paulik, Paulik & Erdey, MOM, Budapest) at the heating rate of 10 K/min. Carbon content was estimated from the mass loss of dry samples (pretreated at 473 K). Hydrothermal treatment of the samples (additionally labeled HTT) was performed in the steam phase at 473 K for 6 h using 5 g of an adsorbent placed in a quartz vessel in a stainless steel autoclave (0.3 dm^3) with 20 ml of water.

2.2. Transmission Electron Microscopy

TEM micrographs of silica gel and carbosil samples (Figs. 1 and 2) were made using a BS 540 (Tesla) apparatus (accelerating voltage 80 kV, resolution 0.8 nm, and magnification ×24000). Microscope samples were prepared using the platinum-carbon replication method with evaporation of platinum and a low amount of carbon onto the adsorbents then treated in hydrofluoric acid to dissolve silica gel.

2.3. Adsorption

Nitrogen adsorption-desorption isotherms (Fig. 3) were recorded at 77.4 K by means of a Micromeritics ASAP 2405N adsorption analyzer. The specific surface area (Table 1, S_{BET}) was computed using standard BET equation (Gregg and Sing, 1982; Adamson and Gast, 1997) at p/p_0 (where p and p_0 denote the equilibrium and saturation pressures of nitrogen, respectively) between 0.06 and 0.2. The pore volume V_p was estimated at $p/p_0 \approx 0.98$ converting the volume of adsorbed nitrogen to the volume of bulk fluid. The average pore diameter (D_p) was calculated for a model of cylindrical pores $D_p = 4V_p/S_{\mathrm{BET}}$. Additionally, the average pore diameter $D_{p,\mathrm{BJH}(a)}$ was determined by the BJH method (Barrett et al., 1951) using the adsorption data. The S_{BET}, V_p, $D_{p,\mathrm{BJH}(a)}$, and D_p values were determined using the standard Micromeritics software.

The specific surface area of micropores at the pore radius $R_p < 1$ nm was calculated using the Dubinin-Stoeckli (DS) equation (Dubinin, 1984; Fenelonov, 1995) applied to the adsorption data at $p/p_0 < 0.2$ with correction related to the adsorption in mesopores. The α_S plots (Fig. 4) (Gregg and Sing, 1982; Adamson and Gast, 1997) were used to estimate the specific surface area of mesopores (S_{mes}) (silica gel Si-1000 was used as a reference material (Jaroniec et al., 1999a, b)). The S_{mes} and S_{BET} values are close; however, sometimes S_{mes} is slightly larger because of both errors in determination of these values and contribution of volume filling of mesopores at $p/p_0 < 0.4$ (since long hysteresis loops are observed in the isotherms (Fig. 3)) leading

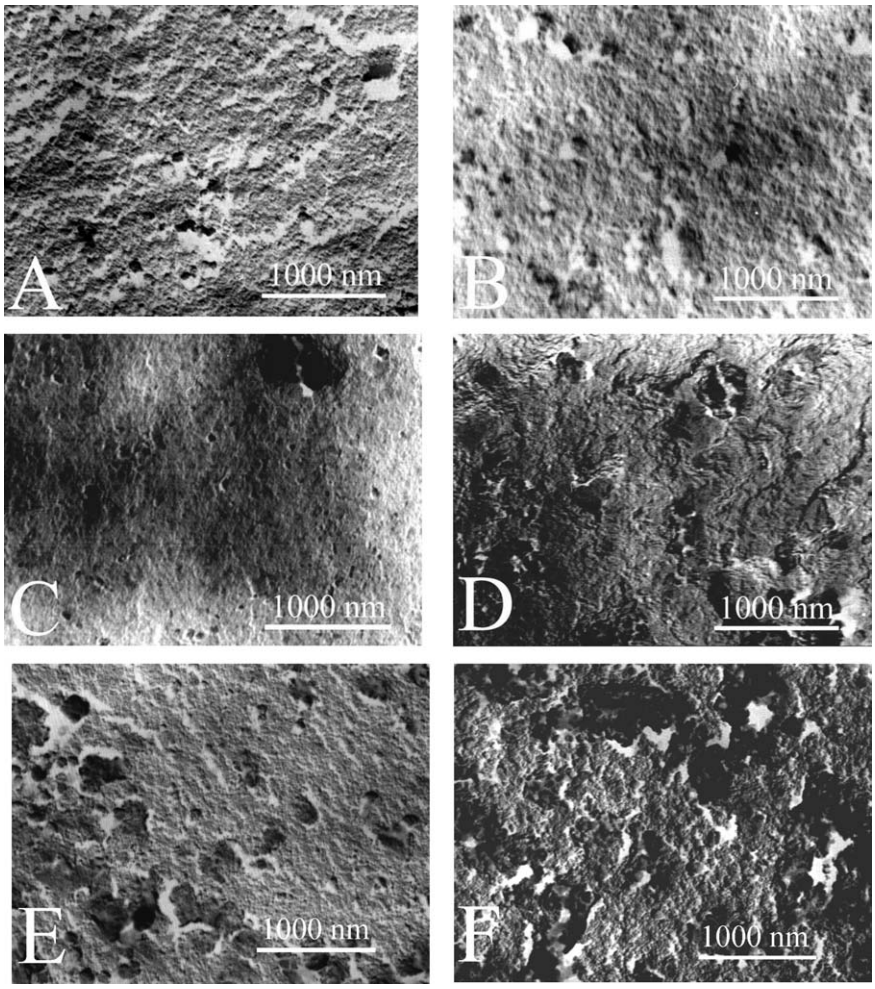

Figure 1. TEM micrographs of (a) Si-60, (b) Si-60-T, (c) CS-1, (d) CS-2, (e) CS-5, and (f) CS-6.

to certain overestimation of S_{mes}. This similarity of the S_{mes} and S_{BET} values depicts nearly pure mesoporous character of all the studied adsorbents.

The specific surface area of pyrocarbon itself (S_C) was determined on the basis of the PNP adsorption (assuming preferable adsorption of PNP onto carbon deposits) from the aqueous solution of hydrochloric acid studied by means of a Specord M-40 (Karl Zeiss, Jena) UV/vis spectrophotometer at 400 nm. The corresponding calculation technique was described in details elsewhere (Kamegawa and Yoshida, 1990, 1993, 1995).

The pore size distributions $f(R_p)$ (Fig. 5) have been calculated using the overall isotherm equation based on the combination of the modified Kelvin equation and the statistical adsorbed film thickness (Nguyen and Do, 1999)

$$a = \int_{r_{\min}}^{r_k(p)} f(R_p)\, dR_p + \int_{r_k(p)}^{r_{\max}} \frac{w}{R_p - \sigma_s/2} t(p, R_p) f(R_p)\, dR_p \quad (1)$$

where $r_{\min}$ and $r_{\max}$ are the minimal and maximal pore radii, respectively; $w = 2$ for cylindrical pores; $r_k(p)$ is determined by the modified Kelvin equation

$$r_k(p) = \frac{\sigma_s}{2} + t(p, R_p) + \frac{w\gamma v_m \cos\theta}{R_g T \ln(p_0/p)} \quad (2)$$

and the statistical thickness $t(p, R_p)$ of an adsorbed layer is computed using the modified BET

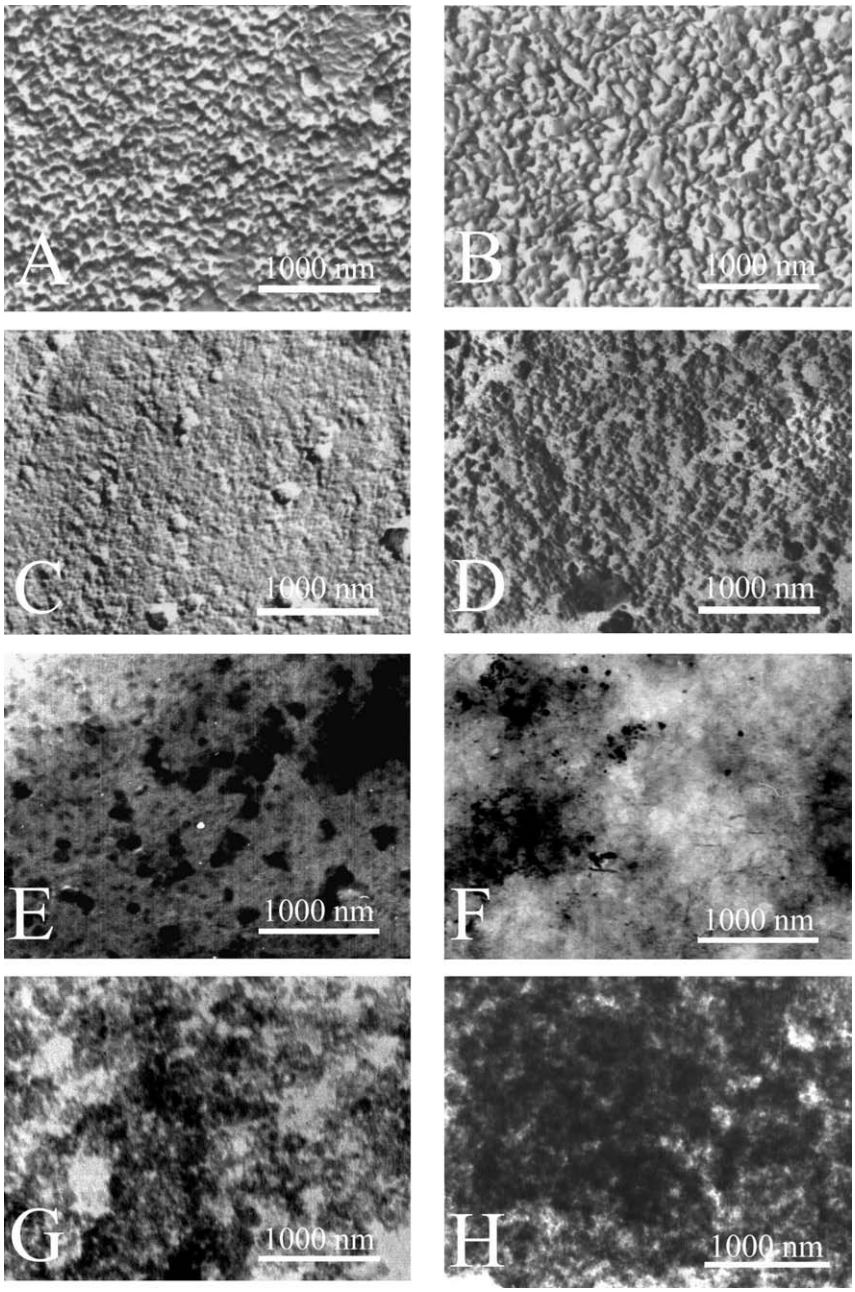

Figure 2. TEM micrographs of (a) Si-60-HTT, (b) Si-60-T-HTT, (c) CS-1-HTT, (d) CS-2-HTT, (e) CS-3-HTT, (f) CS-4-HTT, (g) CS-5-HTT, and (h) CS-6-HTT.

equation

$$t(p, R_p) = t_m \frac{cz}{(1-z)} \times \frac{[1 + (nb/2 - n/2)z^{n-1} - (nb+1)z^n + (nb/2 + n/2)z^{n+1}]}{[1 + (c-1)z + (cb/2 - c/2)z^n - (cb/2 + c/2)z^{n+1}]} \quad (3)$$

$t_m = a_m/S_{\mathrm{BET}}$; $b = \exp(\Delta\varepsilon/R_gT)$; $\Delta\varepsilon$ is the excess of the evaporation heat linked to the interference of the layering on the opposite wall of pores; a_m is the BET monolayer capacity; $c = c_s \exp((Q_p - Q_s)/R_gT)$; c_s is the BET coefficient for the adsorption on a flat surface; Q_s and Q_p are the adsorption heat on flat surface

Table 1. Structural parameters of initial, heated and hydrothermally samples.

Sample	C_C (wt.%)	S_{BET} (m^2/g)	S_C (m^2/g)	S_{mes} (m^2/g)	S_{DS} (m^2/g)	V_p (cm^3/g)	V_{mes} (cm^3/g)	D_p (nm)	$D_{p,BJH(a)}$ (nm)	D_{AJ}
Si-60	–	447		472	25	0.821	0.783	7.3	5.9	2.421
Si-60-T	–	472		509	24	0.867	0.819	7.4	6.1	2.433
Si-60-HTT	–	61		61	20	0.264	0.212	17.2	22.5	2.594
Si-60T-HTT	–	42		42	21	0.126	0.104	12.0	15.2	2.605
CS-1	1.5	431	152	460	19	0.783	0.743	7.3	6.0	2.418
CS-1-HTT		403		406	10	0.829	0.787	8.2	7.2	2.421
CS-2	2.3	458	158	487	27	0.811	0.768	7.1	5.9	2.425
CS-2-HTT		370		373	11	0.808	0.771	8.7	7.7	2.427
CS-3	5.9	445	109	472	28	0.780	0.741	7.0	5.8	2.428
CS-3-HTT		361		361	17	0.733	0.690	8.1	7.2	2.427
CS-4	10.0	427	86	453	30	0.737	0.700	6.9	5.8	2.431
CS-4-HTT		360		365	24	0.676	0.631	7.5	6.5	2.439
CS-5	13.0	399	99	422	31	0.676	0.640	6.8	5.7	2.439
CS-5-HTT		324		320	18	0.622	0.586	7.7	6.9	2.448
CS-6	19.5	354	70	375	27	0.587	0.554	6.6	5.7	2.447
CS-6-HTT		292		286	18	0.535	0.501	7.4	6.7	2.458

Note. C_C is the carbon content; S_{BET} is the specific surface area, S_C denotes the specific surface area of carbon deposits (determined using the PNP adsorption); S_{mes} is the specific surface area of mesopores (linearization of α_s plots at $p/p_0 < 0.4$); S_{DS} is the specific surface area of micropores (DS method); V_p is the pore volume, V_{mes} is the mesopore volume (calculated from $f(R_p)$ at 1.0 nm $< R_p <$ 50 nm using Eqs. (1)–(3); $D_p = 4V_p/S_{BET}$; $D_{p,BJH(a)}$ is the average pore diameter determined by the BJH method (Barrett et al., 1951) using the adsorption data; D_{AJ} is the fractal dimension.

and in pores, respectively; $z = p/p_0$; n is the number (noninteger) of statistical monolayers of adsorbate molecules and its maximal value for a given R_p is equal to $(R_p - \sigma_s/2)/t_m$; and σ_s is the collision diameter of surface atoms (Nguyen and Do, 1999). Desorption data were utilized to compute the $f(R_p)$ distributions with Eqs. (1)–(3) and modified regularization procedure (Provencher, 1982) under non-negativity condition ($f(R_p) \geq 0$ at any R_p) at a fixed regularization parameter $\alpha = 0.01$ using a model of cylindrical pores. Application of this approach to different adsorbents was also described elsewhere (Gun'ko et al., 2001a,b, 2002a–d, 2003).

Calculation of the fractal dimension (D_{AJ}) of the adsorbents was performed on the basis of the adsorption data using adsorption isotherm equation (Avnir and Jaroniec, 1989) at $p/p_0 \leq 0.85$

$$\ln(\Theta) = const + (D_{AJ} - 3)\left[\ln\ln\left(\frac{p_0}{p}\right)\right] \quad (4)$$

i.e., at high coverage when forces of the surface tension at the gas/liquid boundary control the interface and the capillary condensation occurs in mesopores (nitrogen adsorption-desorption isotherms shown in Fig. 3 have marked hysteresis loops).

2.4. ^1H NMR Investigations

The ^{1}H NMR spectra were recorded by means of a WP-100 SY (Bruker) high-resolution NMR spectrometer. Relative mean errors were ±10% for signal intensity and ±1 K for temperature. The technique of freezing-out of water was applied to separate the bulk and interfacial waters in the aqueous suspensions (≈5 wt.%) of silica gel and CS or to distinguish different water layers on the adsorption from the gas phase. The amounts of unfrozen interfacial water (C_{uw}) adsorbed on CS (and silica gel) samples frozen at $180 < T < 273$ K were estimated by comparison of an integral intensity (I_{uw}) of the ^{1}H NMR signal of unfrozen water with that (I_c) of water adsorbed on CS from the gas phase using a calibrated function $I_c = f(C^c)$, assuming $C_{uw} = \frac{C^c I_{uw}}{f(C^c)}$. The function $f(C^c)$ was obtained on the basis of the measurements

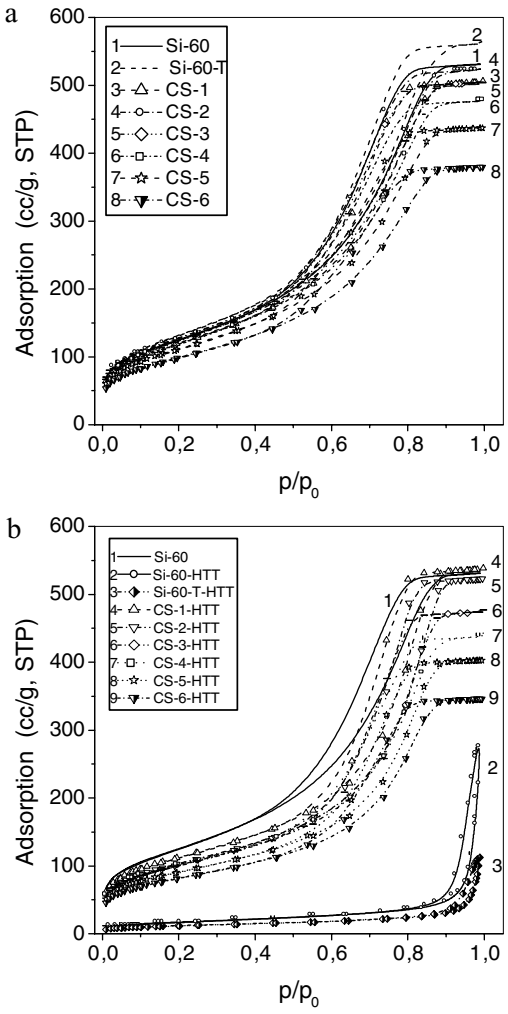

Figure 3. Nitrogen adsorption-desorption isotherms for (a) Si-60, Si-60-T and CS-*i* and (b) hydrothermally treated samples of the first series.

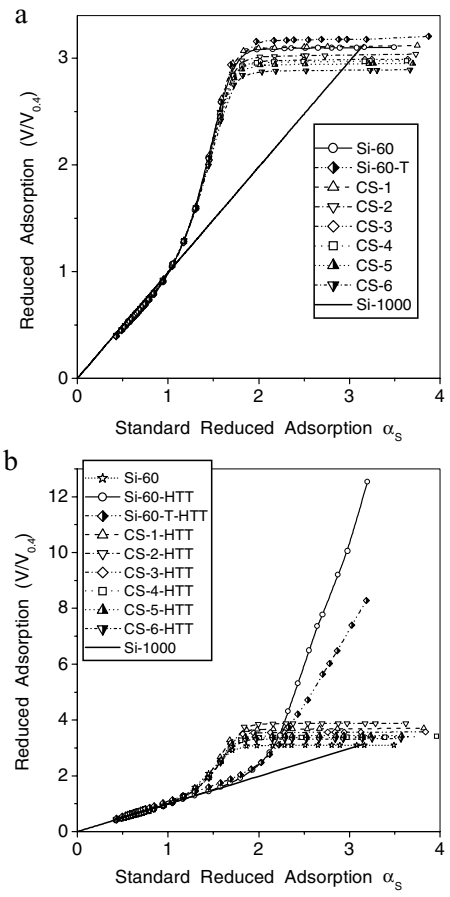

Figure 4. The α_S plots reduced by dividing by the adsorption value at $p/p_0 = 0.4$ for (a) Si-60, Si-60-T and CS-*i* and (b) hydrothermally treated samples of the first series; the α_S plot for LiChrospher Si-1000 silica (used as standard) is shown.

of the integral intensity for given amounts of water (C^c) adsorbed on the CS surfaces from the gas phase. The signals of surface proton-containing groups and water molecules from ice were not detected due to features of the measurement technique and the short time ($\sim 10^{-6}$ s) of cross-relaxation of proton in solids. Changes in the Gibbs free energy (ΔG) of unfrozen interfacial water was calculated (with relative mean error $\pm 10\%$) using the known dependence of changes in the Gibbs free energy of ice on temperature

$$-\Delta G = 0.036(273 - T) \qquad (5)$$

One can assume that water is frozen ($T < 273$ K) at the interfaces when $G = G_i$ and the value of $\Delta G = G - G_0$ is equal to $\Delta G_i = G_i(T) - G_i|_{T=273\,\mathrm{K}}$ and corresponds to lowering of the Gibbs free energy of the interfacial water because of its interaction with the solid surfaces (G_0 denotes the Gibbs free energy of undisturbed bulk water). The used ^{1}H NMR technique with freezing-out of the bulk and interfacial waters was described in details elsewhere (Turov et al., 2002; Turov and Leboda, 1999; Gun'ko et al., 1999; Gun'ko and Turov, 1999). On the basis of this approach, one can calculate the amounts of strongly (C^s_{uw}) and weakly (C^w_{uw}) bound unfrozen waters, a maximal reduction of the Gibbs free energy of strongly (ΔG^s) and weakly bound (ΔG^w) waters, and the Gibbs free energy (γ_S) of adsorption of

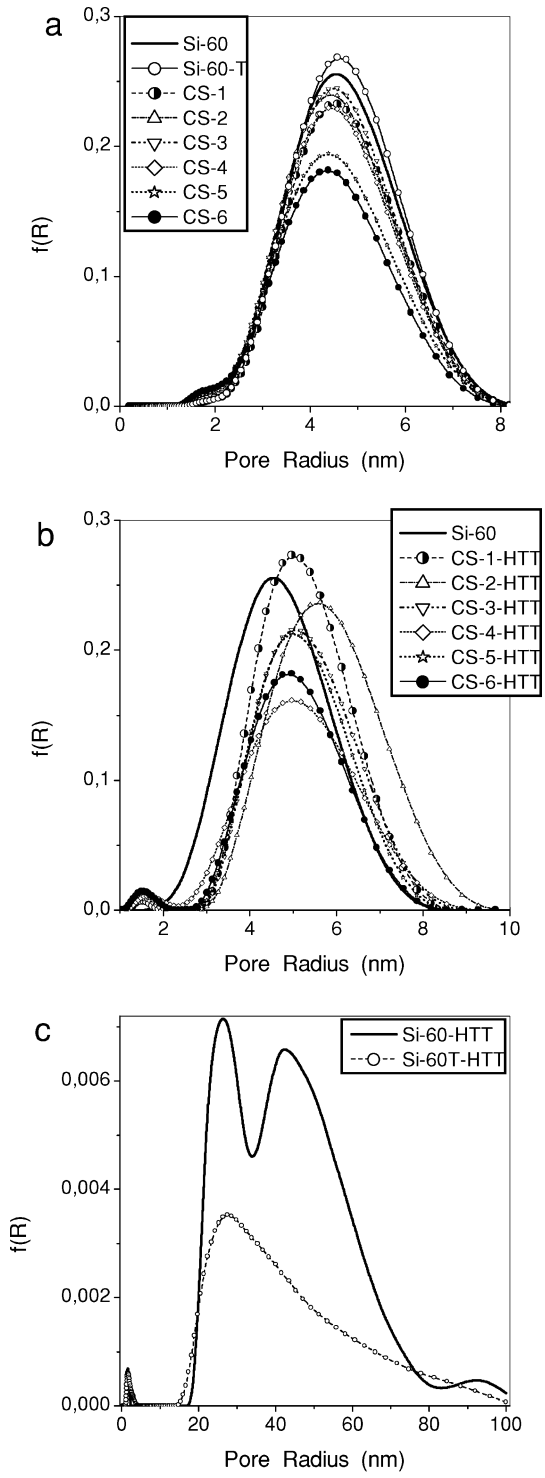

Figure 5. Pore size distributions for (a) Si-60, Si-60-T, and CS-*i*; (b) Si-60 and hydrothermally treated CS-*i* samples; and (c) Si-60-HTT and Si-60-T-HTT at fixed regularization parameter $\alpha = 0.01$.

water unfrozen at $T < 273$ K

$$\gamma_S = K \int_0^{C_{\text{uw}}^{\max}} \Delta G \, dC_{\text{uw}} \tag{6}$$

where $C_{\text{uw}}^{\max}$ is the total amount of unfrozen water at $T \to 273$ K (Turov and Leboda, 1999). Typically the dependence of ΔG on C_{uw} has two portions with significant changes in ΔG at relatively small changes in C_{uw} (corresponding to water strongly bound to adsorbent and placed close to its surfaces as thin water layer) and small changes in ΔG in a large range of C_{uw} (weakly bound water forming relatively thick water layer in mesopores). Linear approximation of these portions of the $\Delta G(C_{\text{uw}})$ graphs towards the intersection with the ΔG axis gives the ΔG^s and ΔG^w values.

3. Results and Discussion

Comparison of the TEM micrographs of Si-60 and CS samples (Fig. 1) reveals that pyrocarbon deposits and the CS surface as a whole become less uniform with increasing carbon content C_C, and the formation of larger pyrocarbon particles occurs mainly at $C_C > 10$ wt.%. However, at low $C_C < 10$ wt.% the carbosil surfaces look relatively uniform (Fig. 1C). Additionally, the surface topography after heating of pure silica gel is akin to that of the pristine oxide (Figs. 1(A) and (B)) (mesopores at $R_p < 10$ nm providing a major contribution to the total porosity of Si-60 are not seen in TEM micrographs). The similarity of the spongy surfaces of Si-60-HTT and Si-60-T-HTT is also observed in their TEM micrographs (Figs. 2(A) and (B)), as well as the similarity in the corresponding nitrogen adsorption isotherms (Figs. 3(b) and 4(b)), the pore size distributions (Fig. 5) and the structural characteristics (Table 1). On the other hand, the differences of CS-*i* and CS-*i*-HTT samples (the latter don't look spongy as pure silica after HTT) are significantly smaller than that for pure silica gel before and after HTT due to shielding of the oxide surfaces by the pyrocarbon layer against decomposition of the silica surface on HTT (Figs. 1 and 2), which reflect in the corresponding differences of the nitrogen adsorption-desorption isotherms (Fig. 3), α plots (Fig. 4), the values of the structural parameters (Table 1), and the pore size distributions (Fig. 5). Thus, substantial changes in the shape of the isotherms (Fig. 3(b), curves 2 and 3) and α plots (Fig. 4(b)) are observed only for pure silica gel after HTT (hydrolysis of the siloxane bonds and mass transferring from

enlarged pores) because of a large difference in the pore size distributions of this sample in comparison with others (Fig. 5). It should be noted that heating of Si-60 at 823 K (Si-60-T) with subsequent HTT (Si-60-T-HTT) gives larger changes in the porosity in comparison with Si-60 (Fig. 5 and Table 1) than that of Si-60-HTT due to the formation of strained siloxane bonds on heating (Kiselev and Lygin, 1972), which can be more easily hydrolyzed than the siloxane bonds on the surface of pristine silica gel.

Pyrocarbon deposits reduce the pore volume and the specific surface area of hybrid adsorbents nearly linearly with increasing C_C (Table 1). However, relative changes $\Delta V_p/V_p$ versus C_C decrease stronger at $C_C > 10$ wt.% (due to blocking of Si-60 pores by carbon plugs) than that on addition of pure ballast (which does not contribute V_p or $S_{\rm BET}$) in contrast to $\Delta S_{\rm BET}/S_{\rm BET}$ (decreasing smaller than $\Delta V_p/V_p(C_C)$ due to contribution of the outer surfaces of pyrocarbon particles possessing, however, very small own porosity) (Fig. 6(a), Table 1). On the other hand at $C_C < 10$ wt.%, the $\Delta V_p/V_p(C_C)$ graph is close to the ballast line (Fig. 6(a)). These effects also reflect in the graphs of the nitrogen adsorption-desorption isotherms for CS-*i* samples (Fig. 3) lowering with C_C but without marked changes in the isotherm and hysteresis loop shapes. Additionally, the reduced (divided by $V_{0.4}$, i.e. amounts of nitrogen adsorbed at $p/p_0 = 0.4$) α_s plots (Fig. 4(a)) are practically independent of the carbon content at $\alpha_s < 1.5$; i.e., changes in the shape of pores on pyrocarbon grafting are relatively small and CS samples remain mesoporous as $S_{\rm BET} \approx S_{\rm mes} \gg S_{\rm DS}$ and $V_p \approx V_{\rm mes}$ (Table 1). Notice that the V_p values are slightly larger than those of $V_{\rm mes}$ due to contribution of macropores at $R_p > 50$ nm. Contribution of micropores to the surface area is very small for all samples (Table 1, $S_{\rm DS}$). Macropores give a larger contribution to the pore volume after HTT, especially in the case of pure silica gel (Fig. 5(c)). Additionally, HTT leads to appearance of narrow mesopores at $R_p < 2$ nm (Fig. 5(b) and (c)) in consequence of pore wall 'pitting'. It should be noted that the $c_{\rm BET}$ values (from standard BET equation) for all the studied samples were between 80 (minimal for Si-60-HTT) and 111 (maximal for CS6-HTT), which are close to that for the initial Si-60 ($c_{\rm BET} = 91$) and CS-*i* (nearly constant between 87 and 88). These small $c_{\rm BET}$ values show a low contribution of micropores to the total porosity for all the samples.

Carbon deposits strongly shield the silica gel surfaces against pore wall disruption on HTT (Figs. 1 and 2) that results in significant differences in the shapes of the isotherms (Fig. (3b)) or α_S plots (Fig. 4(b)), as well as in the $S_{\rm BET}$ and V_p values (Table 1), for CS-*i*-HTT and Si-60-HTT (or Si-60-T-HTT), as the largest alterations in these characteristics are observed after HTT of pure silica gel characterized by strongly enlarged mesopores at $R_p > 20$ nm (Fig. 5(c)). Note that heating of Si-60 before HTT leads to greater changes in the isotherm shape after HTT (Fig. 3(b)) as well as in the V_p and $S_{\rm BET}$ values (Table 1) in comparison with those for Si-60-HTT, perhaps because of the formation of strained Si—O—Si bonds after heating of silica gel, which are more reactive than the siloxane bonds on the surface of pristine silica gel. Consequently, pyrocarbon deposits can tightly cover the silica surfaces

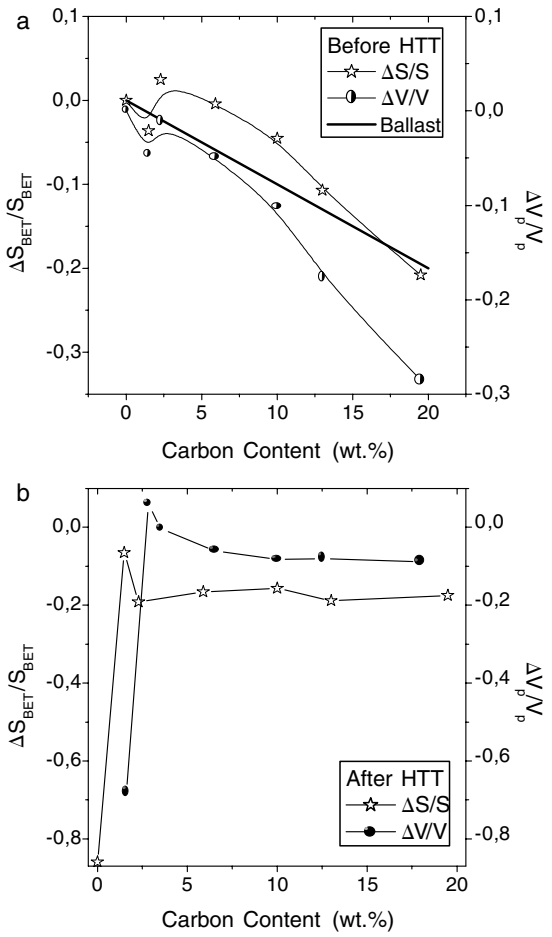

Figure 6. Changes in (a) the pore volume and (b) the specific surface area due to pyrocarbon deposits for carbosils CS-*i* and CS2-*i*; and (c) relative changes in the specific surface area and pore volume due to HTT of CS-*i* samples.

(Fig. 1) even at a low content $C_C = 1.5$ wt.% in CS-1 characterized by reduction of S_{BET} by 6.5% but increase in V_p by 5.9% after HTT, which strongly differ from the corresponding values of pure silica gel after HTT. However, the C_C value in CS-1 is lower than that corresponding to the coverage of total silica gel surface by a carbon monolayer with a continuous graphite sheet. One can assume that strong inhibition of the hydrolysis of the silica gel surfaces during HTT by pyrocarbon deposits (even at low C_C) can be caused not only by blocking of pores by carbon plugs but also by blocking (or transforming) of the most active surface sites (e.g., islands of adjacent hydroxyl groups with formation of Si─O─C or Si─C bonds) in silica gel pores by small graphene clusters. Notice that the activation energy of hydrolysis of the Si─O─Si bonds reduces with increasing number of molecules in the water clusters near these bonds and if Si atoms already have OH groups (Gun'ko et al., 1997, 1998). Pyrocarbon deposits can be non-continuous at low C_C values but they cover active surface sites and can inhibit the formation of adsorption complexes of water that results in the reduction of the hydrolysis rate on HTT. Additionally, the lifetime (Adamson and Gast, 1997)

$$\tau = \tau_0 \exp(E/RT) \tag{7}$$

of water adsorption complexes decreases due to reduction of the energy of the adsorption (E) on the pyrocarbon-covered surfaces possessing lowered hydrophilic properties (Gun'ko and Leboda, 2002; Gun'ko and Bandosz, 2003; Gun'ko et al., 2001b, 2002d). This effect can lead to lowering probability of hydrolysis of the siloxane bonds, i.e. to reduction of the reaction rate.

Pyrocarbon deposits do not practically change a small contribution of micropores (Table 1, S_{DS}), and the reduced α_S plots reveal (Fig. 4(a)) the absence of a significant microporosity of CS as they are close to the reduced α_S plot of Si-1000 at $\alpha_S < 1$. The main $f(R_p)$ peak at $R_p \approx 4$ nm becomes lower and slightly shifts towards smaller R_p values depending on C_C, as the larger the C_C value, the greater the displacement of this $f(R_p)$ peak (Fig. 5(a)). Consequently, a portion of pyrocarbon deposits forms in mesopores, as formation of large pyrocarbon particles (possessing low porosity and specific surface area, Table 1, S_C) on the outer surfaces of silica gel particles (Fig. 1) can case lowering $f(R_p)$ but without the peak displacement (i.e., pyrocarbon deposits which do not possess large own porosity can play a role of the ballast, as the $\Delta V_p/V_p(C_C)$ graph lies close the ballast line at low C_C values (Fig. 6(a)). For CS-i-HTT samples, the main $f(R_p)$ peak shifts toward larger R_p depending on C_C (the smaller the C_C value, the larger the displacement with one exception for CS-2-HTT). The displacement of $f(R_p)$ for CS-i-HTT towards larger R_p in comparison with that for Si-60 and CS-i (Fig. 5) demonstrates that the silica gel pore walls undergo hydrolysis (depending on C_C because of the shielding effect) but substantially less than that for pure silica (Fig. 5(c)). Relative changes in the pore volume and the specific surface area versus C_C of CS-i-HTT (Fig. 6(b)) significantly differ from those of CS-i (Fig. 6(a)). From these dependences, one

Table 2. Characteristics of interfacial water in the aqueous suspension of initial silica gel and carbosils.

Sample	C_C (wt.%)	$-\Delta G^s$ (kJ/mol)	$-\Delta G^w$ (kJ/mol)	C^s_{uw} (mg/g)	γ_S (mJ/m^2)
Si-60	0	3.4	0.8	500	154
Si-60T	0	4.0	1.1	500	119
CS-1	1.5	2.8	0.8	560	124
CS-2	2.3	2.4	0.8	480	127
CS-3	5.9	2.5	1.2	400	116
CS-4	10.0	2.5	1.2	550	109
CS-5	13.0	2.5	0.9	550	137
CS-6	19.5	2.7	1.3	630	164

Note. Superscripts w and s correspond to weakly and strongly bound waters, respectively, unfrozen at $T < 273$ K.

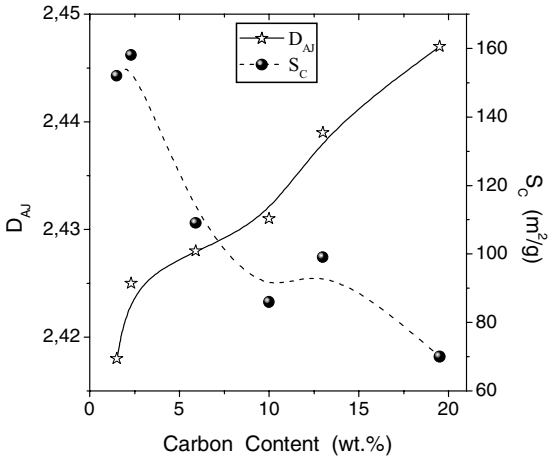

Figure 7. Relationships between the content of pyrocarbon deposits, fractal dimension D_{AJ} and specific surface area of pyrocarbon itself (S_C).

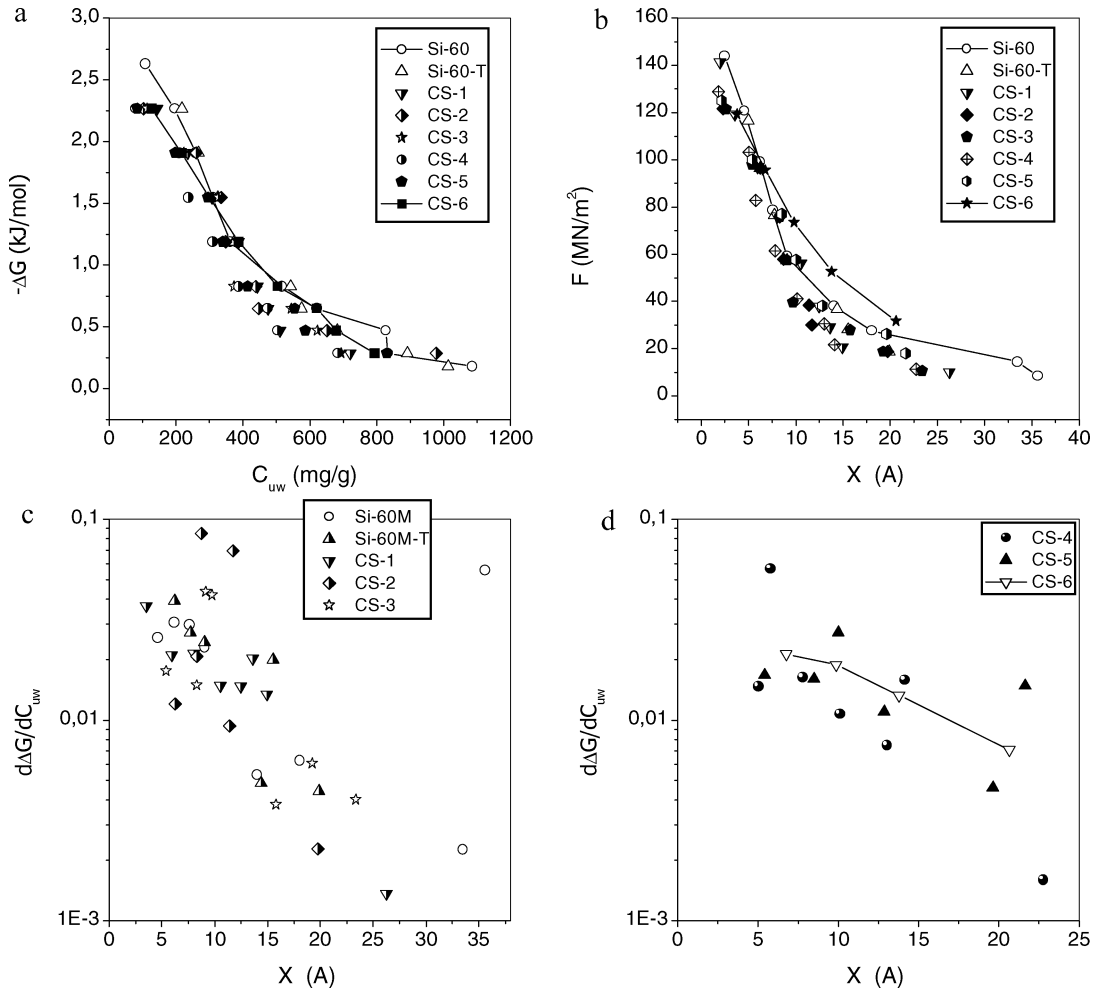

Figure 8. (a) Changes in the free energy of the interfacial water in the aqueous suspension; (b) adhesion forces as a function of the distance X (in Å) to the surface and (c, d) derivatives of ΔG changes in respect to the amounts of unfrozen water as a function of the distance to the surface.

can assume that shielding effect of pyrocarbon slightly decreases with increasing C_C (Fig. 6(b) and Table 1). This may be caused by, at least, two reasons. The first is the segregation of the carbon phase in the form of large particles formed on the outer surfaces of silica gel globules with increasing pyrolysis time (a similar effect was observed on chemical vapor deposition (CVD) of a phase with a low compatibility with a substrate with increasing amounts of the CVD phase (Gun'ko et al., 1999b, 2000b, 2002a)). The second reason is the enhancement of the disorder and the reactivity of the silica surfaces with increasing time of carbonization, since HCl (as a product of CH_2Cl_2 pyrolysis) can react partially (as the carbonization occurs in the flow reactor and a portion of HCl is removed by the nitrogen flow) with silanols and siloxane bonds of the silica surface at 823 K to form ≡SiCl (because of substitution of OH in ≡SiOH for Cl which easily occurs at $T > 623$ K or reaction with ≡Si─O─Si≡ occurring at $T > 770$ K (Tertykh and Belyakova, 1991)) and new ≡SiOH groups. However, the latter processes don't affect a thick silica layer (maybe due to shielding of the silica gel surfaces by pyrocarbon deposits forming Si─O─C and Si─C bonds with the silica surfaces) since carbonization of CH_2Cl_2 causes a small displacement of the main mesopore peak towards smaller R_p values (Fig. 5(a)) and average D_p and $D_{p,\mathrm{BJH}(a)}$ values decreases (Table 1); i.e. disruption of the pore walls of silica gels due to the mentioned reactions is not great on the carbonization of CH_2Cl_2.

An increase in the pyrocarbon content leads to an enhancement of the CS surface roughness (Fig. 1), and fractal dimension D_{AJ} grows nonlinearly with C_C;

however, the specific surface area of pyrocarbon itself (S_C) decreases with C_C (Fig. 7) due to enlargement of pyrocarbon particles (observed in the TEM micrographs). These structural features of CS samples (as well as shielding of active surface sites by pyrocarbon deposits) can impact their adsorptive properties of CS in respect to such a polar adsorbate as water.

The graph shapes of changes in the Gibbs free energy of the interfacial water versus the amount of unfrozen ($T < 273$ K) water ($C_{\rm uw} = C^s_{\rm uw} + C^w_{\rm uw}$) depend on the carbon content only slightly (Fig. 8(a), Table 2) as well as that of adhesion forces F versus the distance X from the surface (Fig. 8b) calculated on the assumption of only radial dependence of F. However, more detailed picture related to the corresponding derivatives $d(\Delta G)/dC_{\rm uw}$ (Figs. 8(c) and 8(d)) and the relationships between ΔG and the characteristics of pores filled by water unfrozen at $T < 273$ K (Fig. 9, Tables 1 and 2) show their deviations from the graphs for pristine Si-60. These deviations reveal an enhancement of the nonuniformity of CS-i samples with increasing C_C also confirmed by the increase in $D_{\rm AJ}$ with C_C (Fig. 7). Lowering of the Gibbs free energy of water adsorbed in narrow pores at $R_p < 4$ nm is maximal for Si-60-T and Si-60 (and Fig. 9(b)), as pyrocarbon deposits are typically less hydrophilic than silica gel surfaces resulting in smaller $-\Delta G$ values for interfacial water at the CS surfaces. Notice that, the energy of water adsorption on non-porous carbon black (similar to studied pyrocarbon) is about 20 kJ/mol, which is significantly lower than the heat of water condensation (≈45 kJ/mol) (Brennan et al., 2001). The steepest changes in ΔG at R_p between 2 and 5 nm (Fig. 9(b)) are related to unfrozen water filling the corresponding mesopores (Fig. 5(a)). The graphs of the surface free energy γ_S and the fractal dimension $D_{\rm AJ}$ as functions of C_C depict their cotrained characters for CS-i samples (Fig. 10), as disturbing of the interfacial water in the confined space of pores and reduction of its Gibbs free energy depends not only on the pore size but also on the roughness of the pore walls (both the pore size and the surface roughness determine the pore + surface fractal dimension) at the same nature of the surfaces (active surface sites). Despite the reduction of S_C with C_C (Fig. 7), the fractal dimension increases with C_C for all the CS-i samples. Therefore, one can assume that the nonuniformity of pyrocarbon deposits increases with C_C (as well as γ_S) and this assumption is in agreement with the TEM micrographs (Fig. 1). However, for materials X/SiO_2 (X = TiO_2, Al_2O_3, GeO_2, and C), the maximal γ_S values

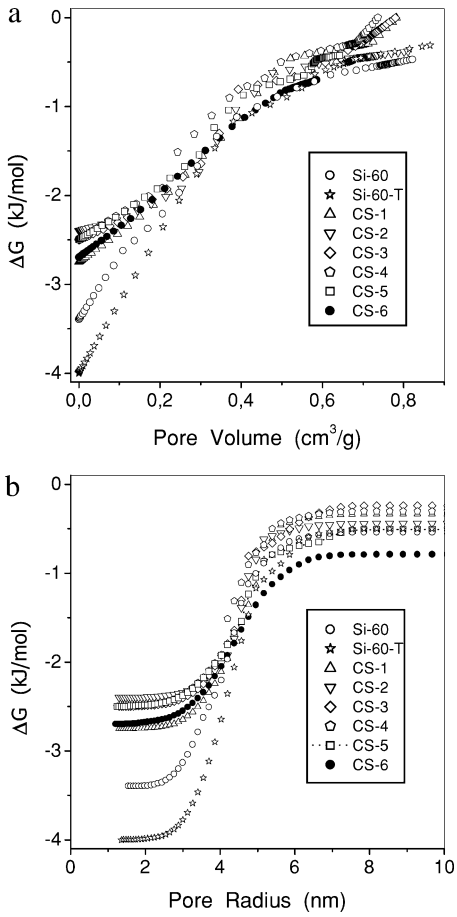

Figure 9. Changes in the free energy of the interfacial water versus (a) the pore volume and (b) pore radius for CS-i.

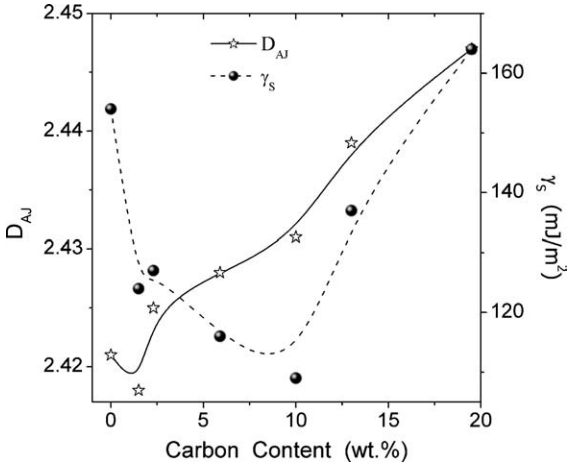

Figure 10. Fractal dimension $D_{\rm AJ}$ and free surface energy γ_S as functions of pyrocarbon content.

were frequently observed at low C_X values (Gun'ko et al., 1999b, 2002d). In the case of strongly nonuniform ternary adsorbents CS_X (X is the second oxide or silicate phase grafted onto the silica matrix) (Gun'ko et al., 2000a), changes in $D_{AJ}(C_{X+C})$ and $\gamma_S(C_{X+C})$ (as well as $D_{AJ}(C_C)$ and $\gamma_S(C_C)$) are complex with large scatter because of a strong impact of both chemical composition of CS_X (possessing a variety of surface active sites), the pore topology and the surface roughness on the structure of the interfacial water, which reflects in the γ_S and D_{AJ} values. Notice that the pyrocarbon structure in CS_X depends strongly on the nature of the X phase (Gun'ko et al., 2000a, 2002c,d).

4. Conclusion

Pyrocarbon deposits reduce the porosity and the specific surface area of CS adsorbents with increasing C_C values, which also affect the pore size distributions. The specific surface area of pyrocarbon itself decreases with C_C. The pyrocarbon layer can be non-continuous but it covers active surface sites and can inhibit adsorption of water that reduces the reaction rate of hydrolysis of the CS surfaces on hydrothermal treatment. Shielding of the silica gel surfaces by pyrocarbon deposits causes significantly smaller structural changes on HTT in comparison with that of pure silica gel. Pre-heating of silica gel at 823 K for 6 h leads to enhancement of the textural changes of pure silica gel on HTT because of appearance of strained siloxane bonds possessing greater reactivity in hydrolysis. Increase in the pyrocarbon content leads to enhancement of the surface roughness, and fractal dimension D_{AJ} of carbon-silica gel adsorbents rises. Changes in the fractal dimension D_{AJ} of CS samples and the Gibbs free energy of the interfacial water γ_S in the aqueous suspensions are concordant in contrast to more complex hybrid adsorbents.

Nomenclature

α	Regularization parameter
a	Adsorption (cm^3/g)
a_m	BET Monolayer adsorption (cm^3/g)
c	BET coefficient
C_C	Content of pyrocarbon deposits (wt%)
c_s	BET coefficient for the adsorption on a flat surface
C_{uw}	Concentration of unfrozen water (wt%)
C^s_{uw}	Concentration of unfrozen water strongly bound to the surfaces (wt%)
C^w_{uw}	Concentration of unfrozen water weakly bound to the surfaces (wt%)
D_{AJ}	Fractal dimension
D_p	Average pore diameter (nm)
$D_{p,BJH(a)}$	Average pore diameter determined using BJH method for adsorption data (nm)
E	Adsorption energy
$\Delta\varepsilon$	Excess of the evaporation heat (kJ/mol)
ΔG	Changes in Gibbs free energy of the interfacial water (kJ/mol)
ΔG^s	Changes in Gibbs free energy of the strongly bound water (kJ/mol)
ΔG^w	Changes in Gibbs free energy of the weakly bound water (kJ/mol)
$f(R_p)$	Pore size distribution
γ	Surface tension (N/m)
γ_S	Module of total changes in the Gibbs free energy of interfacial water (mJ/m^2)
I	Intensity of ^1H NMR signal
I_c	Intensity of ^1H NMR signal of water adsorbed from the gas phase
I_{uw}	Intensity of ^1H NMR signal of unfrozen water at $T < 273$ K
p	Equilibrium pressure (Pa)
p_0	Saturation pressure (Pa)
Q_p	Adsorption heat in pores (kJ/mol)
Q_s	Adsorption heat on flat surface (kJ/mol)
R_g	Gas constant (kJ/K/mol)
R_p	Pore radius (nm)
$r_k(p)$	Pore radius in Kelvin equation (nm)
σ_s	Collision diameter of surface atoms (nm)
S_{BET}	BET specific surface area (m^2/g)
$\Delta S_{BET}/S_{BET}$	Relative changes in the BET specific surface area
S_C	Accessible specific surface area of carbon deposits (m^2/g)
S_{DS}	Specific surface area of micropores determined using DS method (m^2/g)
S_{mes}	Specific surface area of mesopores estimated using the α_S plot method (m^2/g)
Θ	Reduced (a/a_m) adsorption
τ	Lifetime of adsorption complex (s)
T	Absolute temperature (K)
$t(p, R_p)$	Statistical thickness of an adsorbed layer (nm)

t_m	Statistical thickness of a monolayer (nm)
V_p	Pore volume (cm^3/g)
$\Delta V_p / V_p$	Relative changes in the pore volume
V_{mes}	Mesopore volume (cm^3/g)

Acknowledgments

This research was supported by NATO (Grants EST.CLG.976890 and PST.CLG.979895), STCU (Grant No. 1946) and Ministry of High Education and Science of Ukraine (Grant 2M/303-99). R. L. is grateful to the Foundation for Polish Science for financial support.

References

Adamson, A.W. and A.P. Gast, *Physical Chemistry of Surface*, Wiley, New York, 1997.

Avnir, D. and M. Jaroniec, "An Isotherm Equation for Adsorption on Fractal Surfaces of Heterogeneous Porous Materials," *Langmuir*, **5**, 1431–1433 (1989).

Barrett, E.P., L.G. Joyner, and P.P. Halenda, "The Determination of the Pore Volume and Area Distributions in Porous Substances. I. Computations from Nitrogen Isotherms," *J. Am. Chem. Soc.*, **97**, 373–380 (1951).

Brennan, J.K., T.J. Bandosz, K.T. Thomson, and K.E. Gubbins, "Water in porous carbons," *Colloids Surf. A*, **187/188**, 539–568 (2001).

Dabrowski, A. and V.A. Tertykh (Eds.), *Adsorption on New and Modified Inorganic Sorbents*, Elsevier, Amsterdam, 1996.

Dubinin, M.M., "Nonuniform Microporous Structures and Adsorptive Properties of Carbon Adsorbents," *Dokl. AN USSR*, **275**, 1442–1446 (1984).

Fenelonov, V.B., *Porous Carbon*, Nauka, Novosibirsk, 1995.

Gregg, S.J. and K.S.W. Sing, *Adsorption, Surface Area and Porosity*, Academic Press, London, 1982.

Gun'ko, V.M. and T.J. Bandosz, "Heterogeneity of Adsorption Energy of Water, Methanol and Diethyl Ether on Activated Carbons: Effect of Porosity and Surface Chemistry," *Phys. Chem. Chem. Phys.*, **5**, 2096–2103 (2003).

Gun'ko, V.M., A.G. Dyachenko, M.V. Borysenko, J. Skubiszewska-Zięba, and R. Leboda, "CVD-Titania on Mesoporous Silica Gels," *Adsorption*, **8**, 59–70 (2002a).

Gun'ko, V.M., D.J. Sheeran, S.M. Augustine, and J.P. Blitz, "Structural and Energetic Characteristics of Silicas Modified by Organosilicon Compounds," *J. Colloid Interface Sci.*, **249**, 123–133 (2002b).

Gun'ko, V.M. and R. Leboda, "Carbon-Silica Adsorbents," in *Encyclopedia of Surface and Colloid Science*, A. T. Hubbard, (Ed.), pp. 864–878. Marcel Dekker, 2002c.

Gun'ko, V.M., R. Leboda, V.V. Turov, B. Charmas, and J. Skubiszewska-Zięba, "Structural and Energetic Heterogeneities of Hybrid Carbon-Mineral Adsorbents," *Appl. Surf. Sci.*, **191**, 286–299 (2002d).

Gun'ko, V.M. and D.D. Do, "Characterization of Pore Structure of Carbon Adsorbents Using Regularization Procedure," *Colloids Surf. A*, **193**, 71–83 (2001a).

Gun'ko, V.M., R. Leboda, J. Skubiszewska-Zięba, V.V.Turov, and P. Kowalczyk, "Structure of Silica Gel Si-60 and Pyrocarbon/Silica Gel Adsorbents Thermally and Hydrothermally Treated," *Langmuir*, **17**, 3148–3161 (2001b).

Gun'ko, V.M., R. Leboda, J. Skubiszewska-Zięba, and J. Rynkowski, "Silica Gel Modified Due to Pyrolysis of Acetylacetone or Metal (Ti, Cr, Co, Ni, Zn, Zr) Acetylacetonates," *J. Colloid Interface Sci.*, **231**, 13–25 (2000a).

Gun'ko, V.M., R. Leboda, W. Grzegorczyk, J. Skubiszewska-Zieba, M. Marciniak, A.A. Malygin, and A.A. Malkov, "CVD-Titania/Silica Gel Carbonized due to Pyrolysis of Cyclohexene," *Langmuir*, **16**, 3227–3243 (2000b).

Gun'ko, V.M., R. Leboda, B. Charmas, and F. Villieras, "Characterization of Spatial and Energetic Structures of Carbon-Silica Gels," *Colloid. Surf. A*, **173**, 159–169 (2000c).

Gun'ko, V.M., J. Skubiszewska-Zieba, R. Leboda, and V.I. Zarko, "Fumed Silica Carbonized Due to Pyrolysis of Methylene Chloride," *Langmuir*, **16**, 374–382 (2000d).

Gun'ko, V.M. and V.V. Turov, "Structure of Hydrogen Bonds and ^{1}H NMR Spectra of Water at the Interface of Oxides," *Langmuir*, **15**, 6405–6415 (1999a).

Gun'ko, V.M., V.I. Zarko, V.V. Turov, R. Leboda, and E. Chibowski, "The Effect of Second Phase Distribution in Disperse X/Silica ($X = Al_2O_3$, TiO_2, and GeO_2) on its Surface Properties," *Langmuir*, **15**, 5694–5702 (1999b).

Gun'ko, V.M., V.I. Zarko, B.A. Chuikov, V.V. Dudnik, Yu.G. Ptushinskii, E.F. Voronin, E.M. Pakhlov, and A.A. Chuiko, "Temperature-Programmed Desorption of Water from Fumed Silica, Titania, Silica/Titania, and Silica/Alumina," *Int. J. Mass Spectrom. Ion Processes*, **172**, 161–179 (1998).

Gun'ko, V.M., V.V. Turov, V.I. Zarko, E.F. Voronin, V.A. Tischenko, V.V. Dudnik, E.M. Pakhlov, and A.A. Chuiko, "Active Site Nature of Pyrogenic Alumina/Silica and Water Bound to Surfaces," *Langmuir*, **13**, 1529–1544 (1997a).

Gun'ko, V.M., E.F. Voronin, V.I. Zarko, and E.M. Pakhlov, "CVD-Germania on Pyrogenic Silica," *Langmuir*, **13**, 250–259 (1997b).

Jaroniec, M., M. Kruk, and J.P. Olivier, "Standard Nitrogen Adsorption Data for Characterization of Nanoporous Silicas," *Langmuir*, **15**, 5410–5413 (1999a).

Jaroniec, M., M. Kruk, C.P. Jaroniec, and A. Sayari, "Modification of Surface and Structural Properties of Ordered Mesoporous Silicates,"*Adsorption*, **5**, 39–45 (1999b).

Kamegawa, K. and H. Yoshida, "A Method for Measuring Surface Area of carbon of Carbon-Coated Silica Gel," *Bull. Chem. Soc. Japan*, **63**,3683–3685 (1990).

Kamegawa, K. and H. Yoshida, "Carbon Coated of Silica Surface I. Pyrolysis of Silica Gels Esterified with Alcohols," *J. Colloid Interface Sci.*, **159**, 324–327 (1993).

Kamegawa, K. and H. Yoshida, "Carbon Coated of Silica Surface I. Pyrolysis of Silica Gels Esterified with Phenols," *J. Colloid Interface Sci.*, **172**, 94–97 (1995).

Kiselev, A.V. and V.I. Lygin, *IR Spectra of Surface Compounds and Adsorbed Substances*, Nauka, Moscow, 1972.

Leboda, R., "Carbon-mineral Adsorbents—New Type of Sorbents? Part I. The Methods of Preparation," *Mater. Chem. Phys.*, **31**, 243–255 (1992).

Leboda, R., "Carbon-Mineral Adsorbents–New Type of Sorbents. Part II. Surface Properties and Methods of Their Modification," *Mater. Chem. Phys.*, **34**, 123–141 (1993).

Legrand, A.P. (Ed.), *The Surface Properties of Silicas*, Wiley, New York, 1998.

Nguyen, C. and D.D. Do, "A New Method for the Characterization of Porous Materials," *Langmuir*, **15**, 3608–3615 (1999).

Provencher, S.W. "A Constrained Regularization Method for Inverting Data Represented by Linear Algebraic or Integral Equations," *Comp. Phys. Comm.*, **27**, 213–227 (1982).

Tertykh, V.A. and L.A. Belyakova, *Chemical Reaction Involving Silica Surface*, Naukova Dumka, Kiev, 1991.

Turov, V.V. and R. Leboda, "Application of ^{1}H NMR Spectroscopy Method for Determination of Characteristics of Thin Layers of Water Adsorbed on the Surface of Dispersed and Porous Adsorbents," *Adv. Colloid Interface Sci.*, **79**, 173–211 (1999).

Turov, V.V., V.M. Gun'ko, R. Leboda, T.J. Bandosz, J. Skubiszewska-Zięba, D. Palijczuk, W. Tomaszewski, and S. Ziętek, "Influence of Organics on Structure of Water Adsorbed on Activated Carbons," *J. Colloid Interface Sci.*, **253**, 23–34 (2002).

Villieras, F., R. Leboda, B. Charmas, F. Bardot, G. Gerard, and W. Rudzinski, "High Resolution Argon and Nitrogen Adsorption Assessment of the Surface Heterogeneity of Carbosils," *Carbon*, **36**, 1501–1510 (1998).